Assigned tracking number JAD 21-0465.

Journal of Alzheimers Disease

Research article

Porphyromonas gingivalis (W83) infection induces Alzheimer's disease like pathophysiology in obese and diabetic mice

Bojul Bahar[1], Shalini Kanagasingam[2], Murtaza M. Tambuwala[3], Alaa A. A. Aljabali[4], Stephanie A.. Dillon[1], Saeid Doaei[5], Richard Welbury[2], Sasanka S. Chukkapalli[6], Sim K. Singhrao[2*]

[1]Nutrition Sciences and Applied Food Safety Studies, Research Centre for Global Development, School of Sport & Health Sciences, University of Central Lancashire, Preston, PR1 2HE, UK

[2]Brain and Behavior Centre, Faculty of Clinical and Biomedical Sciences, School of Dentistry, University of Central Lancashire, Preston, PR1 2HE, UK

[3]School of Pharmacy and Pharmaceutical Sciences, Ulster University, Coleraine, County Londonderry, BT52 1SA, Northern Ireland, UK

[4]Department of Pharmaceutics and Pharmaceutical Technology, Faculty of Pharmacy, Yarmouk University, Irbid 21163- P.O. BOX 566, Jordan

[5]Saeid Doaei, Research Center of Health and Environment, Shool of Health, Guilan University of Medical Sciences, Rasht, Iran

[6]Department of Oral Biology, College of Dentistry, University of Florida, Gainesville, FL 32610, USA.

*Correspondence to: Sim K. Singhrao at the above address.

Tel: +44 (0) 1772 895137; E-mail: SKSinghrao@uclan.ac.uk

Running Title: *P. gingivalis* infection in a co-morbidity mouse model

Abstract

Periodontal disease and metabolic illnesses negatively impact the quality of life and, eventually, mental health. This study aimed to investigate the effect of *Porphyromonas gingivalis* (W83) oral infection on the development of Alzheimer's disease (AD) pathophysiology in a wild-type obese, diabetic (db/db) mouse model. The db/db mice were either orally infected with *P. gingivalis* and *Fusobacterium nucleatum* or sham infected for 16 weeks. The presence of amyloid-beta (Aβ) and neurofibrillary tangles (NFTs) were assessed using a silver impregnation technique and subsequently by immunohistochemistry for tau and neuroinflammation. The mRNA abundance of a panel of 184 genes was performed using quantitative real-time PCR, and the differentially expressed genes were analyzed by Ingenuity Pathway Analysis. While no Aβ plaques and NFTs were evident by silver impregnation, immunohistochemistry (glial cell markers) of the *P. gingivalis*-infected mice tissue sections exhibited neuroinflammation in the form of reactive microglia and astrocytes. Anti-tau immunopositivity, in addition to cells, was prominent in thickened axons of hippocampal CA neurons. The mRNA abundance of crucial genes in the insulin signaling pathway (*INSR, IGF1, IRS, IDE, PIK3R, SGK1, GYS, GSK3B, AKT1*) were upregulated, potentially exacerbating insulin resistance in the brain by *P. gingivalis* oral infection. Increased mRNA abundance of several kinases, membrane receptors, transcription factors, and pro-inflammatory mediators indicated hyperactivation of intracellular cascades with potential for tau phosphorylation and Aβ release in the same infection group. In conclusion, *P. gingivalis* W83 infection of db/db mice provides a disease co-morbidity model with the potential to reproduce AD pathophysiology with induced periodontal disease.

Keywords: Alzheimer’s disease, diabetes genes, insulin resistance, *Porphyromonas gingivalis*

Introduction

Chronic periodontal disease is one of the most prevalent human chronic diseases that affect the host's immune response and the periodontal tissues, which if left untreated, leads to eventual tooth loss [1]. *Porphyromonas gingivalis* is considered a keystone pathogen of the disease, and is observed in gingival plaque samples of chronic periodontitis patients [2]. The encapsulated serotypes of *P. gingivalis* such as W83 (K1 serotype) are highly effective at causing severe disease because of their ability to stimulate the immune system by inducing several pro-inflammatory cytokines including (IL)-1β, IL-6, IL-17, interferon (IFN)-γ, and tumor necrosis factor (TNF)-α in macrophages and dendritic cells [3]. The pathogenic strains can also directly enter the systemic circulation following toothbrushing of inflamed gingivae [4], as revealed through microbial analysis of the blood samples from the infected host [5]. Lipopolysaccharide (LPS) is also reported to be present in the blood samples of patients with periodontal disease [6]. Growing evidence suggests that periodontopathogens play a role in the modulation of systemic and non-systemic pathological manifestations, especially metabolic syndrome (MetS), which is characterised by the presence of insulin resistance [7] and Alzheimer's disease (AD) [8,9].

AD is a neurodegenerative disease characterised by two microscopical lesions, namely amyloid-beta (Aβ) plaques and intraneuronal neurofibrillary tangles (NFTs) bound to hyperphosphorylated tau protein in the fronto-temporal cerebral cortices [10]. The insoluble Aβ deposition and the development of NFT tau protein have a direct connection with the intracerebral innate immune response and complement activation [11]. Progression and development of Aβ links with microbial infections [12,13], and the inflammatory mediator (cytokines) release that always follows the microbial entry into the host [3,14]. While the role of *P. gingivalis* infection in the development of Aβ deposits is unfolding, it is unclear how the amyloid precursor protein (APP) processing could lead to Aβ deposition.

Numerous studies implicate the association of obesity/type-2 diabetes (T2D) with periodontal disease [15]. Active periodontal disease can potentially affect glycemic control leading to T2D (an example of MetS). T2D patients with periodontitis tend to have fewer teeth, and deeper periodontal pockets containing *P. gingivalis* [16]. The ability of *P. gingivalis* to cause periodontal tissue damage and initiate periodontal pockets is due predominantly to its two main virulence factors, which are gingipains and LPS [17]. LPS mediates the secretion of pro-inflammatory cytokines (IL-1β, IL-6 and IL-8) contributing to hyperglycemia and insulin resistance [18]. Elevated levels of lipid A within the LPS macromolecule can inhibit neutrophil apoptosis and prevent macrophage phagocytosis of

apoptotic cells thereby providing a safe santuary for *P. gingivalis* survival within infected neutrophils [19]. *P. gingivalis* LPS can potentially contribute to the high circulatory level of LPS and is commonly found in individuals suffering from obesity and T2D [7]. Although LPS in blood plasma in MetS is predominantly of gastrointestinal origin [7], the contribution of LPS from *P. gingivalis* in the circulating blood in MetS is likely, but its overall impact remains unclear.

Growing evidence suggests that periodontitis and MetS together exacerbate the onset of AD [20,21]. Currently, longitudinal studies on the intricate association between periodontal disease, MetS and AD are scarce. The obesity/type-2 diabetes (db/db) mouse is a relevant laboratory model for MetS as they develop identifiable obesity around 3-4 weeks of age with an elevated plasma insulin beginning at 10-14 days. Thus, db/db mice provide a valuable co-morbidity model that shows clinical signs of periodontitis and MetS for investigating AD. We initiated the study to test our hypothesis that chronic induction of *P. gingivalis* via the oral route in db/db mice would stimulate the formation of the pathological lesions in the presence of simulated predisposing conditions that co-exitst during AD onset and progression [22-25]. Our main objective in this study was to assess the effect of *P. gingivalis* W83 mediated oral infection on Aβ plaque deposition and NFT formation and to identify the specific molecular pathways that serve as common molecular drivers during inflammation and insulin resistance *in vivo* in db/db mice.

Materials and methods

Mice and infection regime

Obese and type-2 diabetic mice (*db/db* mice) aged five weeks were purchased from Jackson Laboratories, Bar Harbor, MA, USA. Mice at six weeks were randomly assigned to any of the three groups, and periodontal disease was induced by orally infecting with 10^9 colony-forming unit (CFU/ml) *P. gingivalis* W83 (n=9), and *Fusobacterium nucleatum* (ATCC 49256) (n =3) and uninfected (sham mice n=6 as carrier control). The sham mice (sham-infection and /or control group) received the carboxymethyl cellulose (vehicle control) only and the *F. nucleatum* bacterial infection group (an irrelevant bacteria for AD infection was another control group) for the same experimental duration. Mice were orally infected with the capsulated *P. gingivalis* strain W83 (K1 serotype) and *F. nucleatum* and sham, every other week, three times a week for 16 weeks. At the end of the experimental period, mice were

euthanized, and tissues (whole brain, for this study) collected for further analysis. One cerebral hemisphere was fixed in 10% neutral buffered formalin for microscopy and immunohistochemistry and the other cerebral hemisphere was placed into RNA-later and stored at -80ºC for gene expression analysis. Brain samples from AD transgenic Tg2576 mice with the Swedish mutation (n=3) were obtained from Prof. Roxane O. Carare, Faculty of Medicine, University of Southampton, UK, as secondary users of tissue, to act as positive controls for Aβ insoluble plaues and for immunohistochemistry for resident central nervous system inflammatory cell responses.

All experimental procedures were performed in accordance with the guidelines of the University of Florida Institutional Animal Care and Use Committee (IACUC, protocol #201710038) and the University of Central Lancashire, UK (AWERB #RE1718 and RE19/02 (db/bd mice) and RE/17/06 for Tg2576 mice brains).

Light Microscopy

The formalin-fixed brain specimens were processed in an automated tissue processor (Shandon Citadel 2000, Thermo Scientific) and embedded in paraffin wax as per routine methods. The tissue blocks with temporal lobe inclusive of the hippocampus were sectioned (5 mm in thickness) using the Leica RM2235 microtome and collected on Superfrost+® glass microscope slides (Leica UK). Rehydrated paraffin wax sections from the hippocampus of the AD transgenic Tg2576 mice (positive controls) and db/db mice (test specimens) were screened for argyrophilic Aβ1-40/42 insoluble plaques using the modified Methenamine silver stain described previously [26].

Immunohistochemistry

Following dewaxing and acohol dehydration steps, the brain tissue sections from the Tg2576 and the db/db mice were treated with 0.003% H_2O_2 in methanol for 20 min at room temperature to quench endogenous peroxidase activity. The sections were washed in running tap water. For optimal antigen-binding, an antigen retrieval step was included.

Antigen retrieval

Rehydrated paraffin wax sections were optimised for antigen-antibody binding for the calcium-binding protein anti-Iba1 (Invitrogen®, cat no 13269248), which is specifically expressed by microglia, and the glial fibrillary acidic protein (GFAP) expressed by astrocytes

(ab7260, AbCam, UK) using 10mM citric acid buffer (pH 6.1) for 15 minutes at 750W power. Following thorough washings, sections were equilibrated, for 5 minutes, in PBS (0.1M PBS, pH 7.2), and the non-specific antibody binding was controlled by incubating tissue sections for 30 min in blocking solution containing 0.1% normal horse serum (Vectastain kit, PK 4002) in PBS. AD transgenic Tg2576 mice tissue sections acted as positive controls for neuroinflammaton. The negative antibody control sections were incubated in the block solution, whereby the primary antibody was omitted. All other tissue sections were incubated in a humidity chamber, overnight, at 4ºC in the primary antibodies (rabbit anti-GFAP, ab7260, 1/2000) and (rabbit anti-Iba1, 1/150) diluted in blocking solution. The next day, the sections were washed in PBS (x3 for 5 mins each) and incubated for 60 min at room temperature in the biotin labelled anti-rabbit IgG (from kit PK-4001) diluted 1/200 in block solution. From here, the rabbit peroxidase kit (Vector laboratories, Perterborough, UK) and the DAB kit (SK-4100) were used as per manufacturers' instructions. The sections were lightly counterstained in Mayer's haemalum (LAMB/170D) before dehydrating them in graded alcohols and clearing in xylene. The sections were mounted under a coverslip and examined using the Nikon Eclipse E200 Microscope. Images were captured using the DS-L2 v.441 Software (Nikon, UK).

The immunohistochemistry procedure was similar to above for mouse anti-tau (clone AT8, Invitrogen®) except antigen retrieval was omitted. The block solution contained PBS-0.1% triton X-100, horse serum 0.01%) and the mouse anti-tau antibody was diluted 1/20. The secondary detection antibody used was the biotin labelled anti-mouse IgG (from kit PK-4002) diluted 1/200 in block solution.

Gene expression analysis of db/db mice brains

Total RNA extraction

Total RNA was extracted from ~25 mg brain tissue (fronto-temporal) following a two-step procedure. In step 1, the tissue sample was ground in 1 ml TRIzolTM reagent (ThermoFisher Scientific Inc.), and total RNA was obtained following the manufacturer's instructions. In step 2, the purification of the total RNA obtained from step 1 was performed following the GenElute Total RNA Miniprep Kit (Sigma-Aldrich Corp.) according to the manufacturer's instructions. Total RNA was subjected to DNAse I (Sigma-Aldrich Corp.) treatment to

eliminate genomic DNA contamination. Column purification of the RNA was performed using GenElute mammalian total RNA miniprep kit (Sigma-Aldrich Corp.). Total RNA was finally suspended in 50 µl 0.1% diethylpyrocarbonate (DEPC) treated water and stored at −80 °C. The quality and quantity of the total RNA were assessed in a NanoDrop-ND1000 Spectrophotometer (Thermo Fisher Scientific Inc.). The cDNA synthesis was performed with 1 µg of total RNA using the RevertAid H minus first-strand cDNA synthesis kit (Fermentas GmbH, St. Leon-Rot, Germany) following the manufacturer's protocol. The final volume of cDNA was adjusted to 150 µl with nuclease-free water.

Quantitative real-time PCR (qPCR) array

The expressions of a panel of 192 genes were evaluated using a custom-designed qPCR array (Thermo Fisher Scientific Inc), performed in a QuantStudio 5 real-time PCR system (Applied Biosystems). The qPCR arrays (96-well format x 2) enabled mRNA screening of a total of 184 target genes and eight internal controls. The target genes screened included the common markers of the inflammatory immune cascade, oxidative stress, glucose metabolism and insulin pathways. This panel of genes was previously used to capture the intracellular signalling pathways associated with the chronic inflammation induced by *P. gingivalis* LPS treatment [27]. For the qPCR array run, 25 µl cDNA (after 1:5 dilution) from each replicate within a single treatment group were pooled. The qPCR was performed on a 20 µl reaction mixture per well containing 1 µl pooled cDNA, 9 µl water and 10 µl SYBR green master mix (Applied Biosystems). The thermal cycling conditions were 94 °C for 30 s, followed by 60 °C for 1 min, for 40 cycles. In this experiment, a CT value of 35 was considered as the cut-off limit. The relative quantities (2–ΔCt) of the target genes were normalized using the geometric mean of the relative quantities of three internal control genes (beta-actin (ACTB), hypoxanthine-guanine phosphoribosyl transferase 1 (HPRT1) and beta-2 microglobulin (B2M). Briefly, average ΔCt was calculated as the difference of Ct values of any target gene minus the geometric average of the Ct value of the three reference genes. Then, fold change was calculated as 2(− average ΔCt target gene)/2(− average ΔCt reference gene). The differentially expressed genes between any two treatments were identified from the ratio of fold change values with a cut-off ± 1.8 fold.

Gene Ontology and Pathway Analysis

Gene ontology (GO) of the differentially expressed genes was performed using the database for annotation, visualization and integrated discovery (DAVID), a web-based online

(http://david.abcc.ncifcrf.gov/) bioinformatics tool [28]**.** The major annotation clusters of GO term were identified based on the enrichment score calculated by the DAVID tool's default setting. For pathway analysis, the fold change values were analyzed using Qiagen Ingenuity Pathway Analysis (IPA) and the relevant canonical pathways were identified using the default setting in the software. The statistical probability (*P*-value) of the observed number of genes affecting a particular biological function was calculated based on Fisher's Exact Test. This *P*-value indicated the statistical probability of the observed number of genes affected out of the total number of genes evaluated in the PCR array for the biological function. The correlation between the relationship direction and gene expression was determined by calculating the Z-score following the formula $Z = (N+ - N-)/\sqrt{N}$ where N+ represents the number of genes whose expression follows the same direction while N− represents the number of genes whose expression follows an opposite direction of the expression of a particular gene compared to that already available in the IPA knowledge database. N indicates the total number of genes affected. A high stringency Z-score between ≥+2.0 or ≤− 2.0 was applied to identify the most relevant signalling pathways.

Results

Brain histology

Haematoxylin and Eosin morphology staining of the formalin fixed, paraffin wax embedded and rehydrated temporal lobe tissue sections from Tg2576, *P. gingivilas* W83, *F. nucleatum* infected and sham mice showed they were well preserved (not shown). Silver impregnation of the tissue sections from the Tg2576 mouse brains demonstrated numerous Aβ plaques, which were of variable sizes, randomly distributed, within the fronto-temporal cortices including the hippocampus (Fig. 1a). The argyrophilicAβ plaques and NFTs were absent in the hippocampus or in the fronto-temporal cortices of db/db brain tissue sections, from the *P. gingivilas* W83, *F. nucleatum* infected and sham mice groups (Fig. 1b-d).

Immunohistochemistry

Neuro inflammation

Microglosis

The negative controls whereby the primary antibody was omitted remained negative (Fig. 2a-d). In theTg2576 mice (Fig. 2e arrows), and the sham (Fig. 2f arrows) and the *F. nucleatum* infected (Fig. 2g arrows) activated microglia were below the threshold of the numbers (not counted) observed in the *P. gingivalis* W83 infected mice brain tissue sections (Fig. 2h and I arrows).

Astrogliosis

Anti-GFAP immunostaining of the AD trangenic Tg2576 mice brain sections demonstrated the presence of abundant, reactive, astrocytes in close vicinity to the Aβ plaques (Fig 3a box, b, where p represents the $A\beta_{1-42}$ plaque core and is the area within the box from Fig. 3a). The sham-infected mice brain tissue sections (Fig. 3c box, d area within the box in 3c) demonstrated resting astrocytes. *F. nucleatum* infected mouse hippocampus demonstrated significant numbers (not counted) of activated, astrocytes (Fig. 3e box, f area within the box in 3e). The *P. gingivalis* W83 infected mice brain tissue sections (Fig. 3g area within the smaller box is represented in h and i is the are area from the larger box in 3g) also demonstrated an abundance of reactive astrocytes almost equivalent (not counted) to those observed in *F. nucleatum* infected mice tissue sections (Fig. 3e, f).

Mouse anti-tau (AT8) immunostaining for detecting neurofibrillary tangles

As expected, the AD trangenic Tg2576 mice exhibited an intense immunopositive staining for tau within numerous CA neuronal cell bodies. The axon hillock of some neurons was also immunostained (Fig. 4a arrows). Overall the tau staining in the sham (non-infected) group of mice was weak (Fig. 4b and arrow). In the *F. nucleatum* mice, a weak tau immunostaining was observed within the CA neurons without evidence of staining within the axon hillocks (Fig. 4c). The *P. ginivalis* W83 infected mice demonstrated tau immunostaining within the CA neurons (Fig. 4d) and equally stronger tau positivity within thickened bundles of axonal hillocks in the hippocampal CA neurons (Fig. 4e boxed area shown in f, arrows point to thickened axonal hillocks).

Gene expression in brains using qPCR array

Of the total 192 genes evaluated on the qPCR array, the mRNA of 184 genes were detectable. The mRNA abundance of a total of 96 genes in the cerebral hemisphere was differentially

expressed due to the *P. gingivalis* W83 induction of obese diabetic mice (Table 1). The primary group of genes upregulated (by >2 fold) by *P. gingivalis* W83 infection within the extracellular space of the cells includes the growth factor *IGF1* and several cytokines (*IL1A*, *IL1B*, *CSF1*, *LTA* and *CXCL1*0). Other genes upregulated in the extracellular space include *IGFBP3*, *CRP* and *RETN*. In the plasma membrane, genes upregulated include transmembrane receptor (*IGF1R, TLR4*, *TLR6, ICAM1*, *VCAM1*, *IL6R, IL1R2, CD28, CD80*), G-protein coupled receptor (*ADORA1, CCR2, GLP1R, GLP2R*) and membrane transporters (*LDLR*). Besides, the mRNA abundance of two crucial kinases (*INSR, KDR*) and plasma membrane-associated enzymes (*ACE, ADA, DPP4, PTPRC*) and other molecules (*DOK2, CLTC, MYD88, CAP1*) were also upregulated by >2 fold. As expected, within the cytoplasm, the major group of molecules affected were kinases (*AKT1, PIK3R1, PIK3R2, PRKCA, PRKCB, PRKCD, JAK2* etc.) and enzymes (Table 1). The mRNA abundance of 12 transcription factors (*FOXO1, NFKB2, NFATC2, CTNNB1, FOS, SREBF1, SREBF2, TRP53, STAT3, JUN, SMAD7* and *CBL*) were also upregulated whilst two transcription factors (*CREB1* and *STAT6*) were down-regulated. Other genes differentially expressed within the nucleus included ligand-dependent nuclear receptor (*NR4A2*), nuclear kinase (*GSK3B*), enzymes (*APC, AEBP1*) and other molecules (*CDC27*).

Annotation clustering and gene ontology

An evaluation of the panel of differentially expressed genes revealed the major annotation clusters and gene ontologies associated with the molecular, biological and cellular processes altered in the cerebral hemisphere of the db/db mice induced with *P. gingivalis* W83. A total of 13 annotation clusters with an enrichment score of ≥2.0 were scored, of which four most relevant clusters with the highest scores are presented in Table 2. Cluster 1 (enrichment score 7.97) includes the well-represented gene ontology (GO) terms relating to protein phosphorylation, kinase activity, transferase activity, intracellular signal transduction, ATP binding and nucleotide bindings indicating that the genes differentially expressed by the *P. gingivalis* W83 induction are likely to affect these intracellular processes (Fig. 5a). Cluster 2 (enrichment score 4.06) relates to the inflammatory immune response (Fig. 5b). Two other highly enriched annotation clusters (Cluster 3 and 4) include GO terms relating to insulin and insulin receptor signalling pathways (Fig 5c and 5d).

Intracellular Pathways affected in *P. gingivalis* infected db/db mice

The list of most relevant intracellular signaling pathways and the number of gene affected within each of these pathways due to *P. gingivalis* W83 induction of mice versus *F. nucleatum* and sham control groups are presented in Table 3. The pathway analysis revealed that classical signaling associated with inflammatory immune response (NF-kB signaling, neuroinflammatory signaling, toll-like receptor signaling, LPS mediated MAPK signaling, IL1 and IL6) upregulated in the *P. gingivalis* W83 infected mice brains. Besides, pathways for cell growth, survival and proliferation (IGF-1 signaling, PI3K/AKT, PTEN and mTOR signaling pathways) and cellular metabolism and insulin signaling (PPAR, insulin receptor signaling, insulin secretion pathways and T2D signaling) were affected in the *P. gingivalis* W83 induced mice. As expected, these pathways were mostly unaffected when assessed in sham and the *F. nucleatum* control mice.

Discussion

This study aimed to investigate the effect of *Porphyromonas gingivalis* (W83) oral infection on the development of AD pathophysiology in an obese, diabetic (db/db) mouse model. The Aβ insoluble plaque hallmark of AD in a wild-type young mouse model of periodontitis following an oral infection with the highly virulent strain of *P. gingivalis* W83 (capsular K1 serotype) has been previously reported [29]. This was the first report which demonstrated classical human AD look-alike Aβ plaque deposits in the hippocampus of a mouse model of periodontal disease, which would be expected to be demonstrated by neutral histology stains such as silver impregnation used in the present study.

Encouraged by the Ilievski et al. [29] data, and based on the knowledge that periodontal disease, cardiovascular disease, diabetes (MetS) represent a greater risk of dementia for individuals who have suffered multiple co-morbidities in their lives [8,9,22,23,30], we used a co-morbid disease db/db mouse model to reproduce the cardinal hallmark lesions of AD, following an oral infection with the same strain of *P. gingivalis* (W83) [29]. However, in db/db mice, the classical AD Aβ plaques and NFT formation were not observed in the hippocampus or any other anatomical regions of the brain following the silver impregnation of tissue sections. Regarding anti-tau immunostaining, our observations are similar to the Díaz-Zúñiga et al. [14] study in which oral infections of rats with several capsular *P. gingivlis* strains of variable serotypes and virulence showed the absence of the

classical AD Aβ plaques shown by Ilievski et al. [29]. An underlying reason behind the lack of Aβ deposition in the present study could be that the mice were obese and of diabetic dispostionand not of healthy wild-type phenotype. A high level of circulating insulin is a hallmark of insulin resistance and could prevent Aβ and NFT accumulation [31]. Insulin can potentially increase the activities of anti-amyloidgenic proteins such as insulin-degrading enzyme (IDE) and inhibit the phosphorylation of tau by glycogen synthase kinase-3b (GSK3B) activity [31,32]. This led us to change the course of our investigation into gene array methodology for early clues to AD pathophylogical changes in the oral infection mediated periodontal model for AD.

However, before moving on, Díaz-Zúñiga et al. [14] observed thickened axons in the hippocampal neurons of *P. gingivalis* (capsular forms) infected rat brains which they suggested were equivalent to the human AD NFT lesion [14]. In the present study, following anti-tau immunostaining we also observed thickened axon hillocks of cortical hippocampal neurons reported by Diaz-Zuniga et al. [14], which contrasts with the explanation offered by Pandini et al [31] and Cholerton et al. [32]. Díaz-Zúñiga et al. [14] and Ilievski et al. [29] also observed neuroinflammation with the capsulated *P. gingivalis* strains as originally reported by Poole et al. [33] in their *P. gingivalis* (strain 381, non-capsulated, K0 serotype) mono-infected apolipoprotein knockout mouse model. In the db/db mouse model, *F. nucleatum* infected mouse hippocampi demonstrated significant numbers of activated, astrocytes but not microglia. This was an interesting observation showing that even a non-pathogenic bridging bacterium like *F. nucleatum* can stimulate astrocytes but a stronger immune stimulation from the pathogenic *P. gingivalis* W83 infected mice brain tissue sections demonstrated abundant reactive microglia. All these reports confirm that an oral infection with *P. gingivalis* in rodents always leads to an inflammatory intracerebral episode as in humans after an infectious episode [34] which has been associated with cognitive deficit [35].

When we evaluated the gene expression analysis of a panel of 184 genes that were altered due to *P. gingivalis* (W83) oral infection, we observed that the pathways of insulin signaling and neuroinflammatory immune response mediated by PI3K/AKT1 were hyperactivated in the brain in response to the *P. gingivalis* infection demonstrating the potential of *P. gingivalis* W83 induced co-morbidity in the mice model of AD.

In the present study, the *P. gingivalis* infection mediated the activation of insulin secretion, insulin receptor signalling, and IGF-1 signalling pathways. These interconnected

pathways involve multiple signalling routes, potentially contributing to AD pathophysiology (Fig. 6). The mammalian brain, a highly insulin-sensitive organ, heavily depends on insulin to utilise glucose as an energy source and support cognitive functions [36]. Endogenous insulin released by the pancreas crosses the blood-brain barrier to enter the neural tissue of the brain but our results suggest a plausible activation of a localised insulin secretion in the hippocampus following the *P. gingivalis* infection. Our gene expression pathway analysis identified 11 genes (*GLP1R, INSR, JAK2, PIK3R1, PIK3R2, PRKACA, PRKAR1A, PRKCA, PRKCB, PRKCD* and *STAT3*) whose mRNA abundance indicated activation of a localised insulin secretion mechanism in the hippocampal region. One potential route of insulin secretion in the brain is via glucagon-like peptide 1 (GLP-1) and protein kinase [37]. During a hyperglycemic state, GLP-1 in the brain is able to cross the blood-brain barrier [38] and inhibit glucose utilisation and cause insulin secretion [39,40]. In this study, *P. gingivalis* induction resulted in a higher mRNA abundance of *GLP1R* and several kinases and their receptors and lower mRNA abundance of *G6P*, a key glucose utilisation marker. The adult neuronal cells of the hippocampus were previously reported to secrete insulin [41]. A localised synthesis of insulin in the brain may be a compensatory mechanism linked to the insulin resistance that has the potential to develop following *P. gingivalis* infection and its mechanims of action warrants further research.

AD is a neurodegenerative disease being linked to MetS often characterised by insulin resistance, oxidative stress and neuroinflammation [42-44]. As identified through pathway/GO analyses, a higher level of insulin activity in the brain potentially causing insulin resistance was also evident from the increased mRNA levels of key markers of the insulin/insulin-like growth factor-1 (IGF-1) pathways. For example, the *P. gingivalis* infection increased the mRNA abundance of *IGF1*, insulin receptor (IR), IGF-1 receptor (*IGF1R*) and IGF binding protein (*IGFBP3*) genes. While the shared IR/IGF1R system in the plasma membrane of hippocampal cells is crucial for normal insulin signalling. Binding of IGFBP-3 to IGF-1 can potentially contribute to glucose intolerance and insulin resistance in the brain [45]. An interesting protein in the IR/IGF1R system is the insulin receptor substrate 1 (IRS-1), a docking protein, which is a primary checkpoint for the insulin signalling pathway and glucose metabolism regulation [42]. The normal physiological activation of the insulin signalling is achieved by binding insulin to the insulin receptor within the extracellular matrix resulting in the phosphorylation of IRS-1 at the tyrosine residue. However, phosphorylation on multiple serine residues can inhibit IRS-1 activity and result in insulin resistance [46]. *P.*

gingivalis infection increased the mRNA abundance of the *IRS1* gene. Whether an increased level of *IRS1* mRNA due to the *P. gingivalis* infection in this study is associated with phosphorylation at the serine residues, thereby contributing to the insulin resistance requires further investigation.

The interaction of insulin/IGF-1 to the IR/IGF1R receptor system triggers the release of IRS-1/2 and subsequent activation of the phosphatidylinositol 3-kinase type I (PI3K)/AKT pathways [42]. Our gene expression profiling indicated *P. gingivalis* infection activates multiple pathways that potentially lead to hyperactivation of the PI3K/AKT pathway genes. These include numerous mRNA markers of the IR/IGF1R, LPS/TLR and MAPK pathways (Fig. 5). The PI3K/AKT1 pathway plays a vital role in the metabolism of nutrients and maintains cellular homeostasis essential for cell growth, survival and differentiation [47].

An impaired insulin/PI3K/AKT1 pathway activity can contribute to the onset of neurodegenerative diseases [47,48]. During the cellular oxidative stress, PI3K, together with AKT1, triggers reactive osygen species (ROS) production [49,50]. The hyperactivation of PI3K/AKT pathway resultes in lower nitric oxide (NO) production, higher ROS activities, and a higher level of pro-inflammatory cytokines, which are known to culminate in the pathophysiology of AD [42]. A conspicuous decrease in the mRNA abundance of nitric oxide synthase 2 (NOS2) by *P. gingivalis* infection observed in this study further suggests potentially a lower level of NO synthesis. Other mechanisms of AKT-mediated response include affecting glucogenesis, lipolysis and mTOR-mediated protein synthesis, leading to impaired autophagy and synaptic plasticity associated with AD pathophysiology [48]. The pathway analysis also revealed inhibition of the phosphatase and tensin homolog (PTEN), a tumour suppressor molecule that catalyses the conversion of PIP3 to PIP2 and reverses the PI3K/AKT activities. Inhibition of the PTEN pathway is likely to contribute to the hyperactivation of PI3K/AKT pathways.

In the present study, the mRNA abundance of *AKT1* and its three crucial downstream cascades triggered by the action of *GSK3B, FOXO1* and *NFKB2* genes as they were upregulated by *P. gingivalis* infection. Hyperactivity of AKT1 may lead to excessive phosphorylation of GSK-3B, FOXO1 and NF-kB, resulting in several consequences that affect metabolic and cognitive functions [47]. AKT1/GSK-3B hyperactivation causes abnormal phosphorylation of tau, leading to neurofibrillary tangle formation, a hallmark of AD pathophysiology [42,51]. In this study, the mRNA abundance of both *AKT1* and *GSK3B* genes were increased by the *P. gingivalis* infection, and a higher level of phosphorylated tau

was also evident in the hippocampal neurons with thickened bundles of axon hillock(s) in the hippocampus. *P. gingivalis* infection inducing greater phosphorylated tau was also reported by other recent studies [29,52]. AKT1/GSK-3B hyperactivation can also promote a pro-inflammatory state through phosphorylation of STAT3. This transcription factor is required to induce pro-inflammatory cytokines [53], and its mRNA abundance was also increased confirming previous reports for *P. gingivalis* infection mediated cytokine release [3]. We have previously demonstrated that *P. gingivalis* LPS increased the mRNA abundance of *GSoK3B, STAT3* and *CREB1* genes in the IMR-32 neuronal cell model [27]. In this study, while the mRNA abundance of *GSK3B, STAT3* genes increased due to *P. gingivalis* infection, that of *CREB1* gene decreased. The *P. gingivalis* mediated induction of pro-inflammatory responses is likely to include LPS and gingipain virulence factors [9], and it is a multi-component signaling cascade that is likely to be induced that may negatively impact on tau hyperphosphorylation.

The activation of the AKT1/FOXO1cascade results in enhanced transcriptional activity of FOXO1 that can lead to hyperglycemia and ROS production, and thus insulin resistance and oxidative stress [54]. FOXO1 can also activate c-Jun N-terminal kinase and inhibit Wingless (Wnt) pathways and can contribute to Aβ plaque formation and phosphorylation of tau, potentially leading to neurodegeneration [54]. The FOXO1 within the nucleus activates the transcription of many inflammatory mediators. In the present study, the mRNA abundance of FOXO1, and that of a few downstream molecules such as pro-inflammatory cytokines (*IL1B*), wound healing factor (*VEGF*), and adhesion molecule (*VCAM1*) were increased. Together these observations suggest that *P. gingivalis* infection does indeed hyperactivate the AKT1/FOXO1 cascade, and could potentially exacerbate the insulin resistance and oxidative stress pathways.

In the present study, the mRNA abundance of the NF-kB cascade (*NFKB2, IKBKB*) and pro-inflammatory cytokines (*LTA, IL1A, IL1B, IL6R, CSF1*) were upregulated by the *P. gingivalis* infection. The AKT1/NF-kB signaling plays a crucial role in the inflammatory response, oxidative stress, activation of microglia, and apoptotic cell death, thereby contributing to neurodegeneration [55]. The NF-kB has both neuroprotective and neurodegenerative roles in AD. One of the mechanisms through which NF-kB contributes to AD is mediated by activation of βsite APP cleaving enzyme 1 (BACE1). An excessive cleavage of amyloid-beta precursor protein (A□PP) leads to A□ plaque deposition [56]. The gene expression pathway analysis further indicated that the PPAR pathway was down-

regulated due to the *P. gingivalis* infection in db/db mice. Inhibition of PPAR activities may, therefore, lead to the higher activity of BACE1 [57].

Individuals with periodontal disease have an increased risk for cardiovascular pathologies and AD. Subjects with predisposing factors like MetS, obesity and diabetes, are at greater risk of developing periodontal disease and AD [58]. The db/db mouse model tested here provided a unique opportunity to explore the associations between obesity, diabetes and periodontitis on the development of AD. Our observations from the present study provides further support to the notion that AD is an inflammatory disease affected by peripheral (systemic) [23,59,60], and intracerebral inflammatory events which ultimately impact on cognitive decline [61,62].

Disclosure statement

The authors declare no competing interests.

Funding

SK and SKS in 2017 and again with BB and RW and SKS in 2018 received PreViser awards from the Oral and Dental Research Trust. In addition, SK also acknowledges having received a TC White Young Researcher award (2019). SC acknowledge the support from faculty seed grant (UFCD), University of Florida, gainseivlle, Flroida,USA.

References

1. Chapple IL, Van der Weijden F, Doerfer C, Herrera D, Shapira L, Polak D, Madianos P, Louropoulou A, Machtei E, Donos N, Greenwell H, Van Winkelhoff AJ, Eren Kuru B, Arweiler N, Teughels W, Aimetti M, Molina A, Montero E, Graziani F (2015) Primary prevention of periodontitis: managing gingivitis. *J Clin Periodontol* 42 Suppl 16:S71-6. doi: 10.1111/jcpe.12366
2. How K, Song K, Chan K (2016) *Porphyromonas gingivalis*: An Overview of Periodontopathic Pathogen below the Gum Line. *Front microbiol.* 7. 53. doi: 10.3389/fmicb.2016.00053.
3. Vernal R, León R, Silva A, van Winkelhoff AJ, García-Sanz J, Sanz M (2009) Differential cytokine expression by human dendritic cells in response to different porphyromonas gingivalis capsular serotypes. *J Clin Periodontol* **36(10),** 823-829.
4. Silver JG, Martin AW, McBride BC (1977) Experimental transient bacteraemias in human subjects with varying degrees of plaque accumulation and gingival inflammation. *J Clin Periodontol* **4(2),** 92-99.

5. Païssé S, Valle C, Servant F, Courtney M, Burcelin R, Amar J, Lelouvier B (2016) Comprehensive description of blood microbiome from healthy donors assessed by 16S targeted metagenomic sequencing. *Transfusion* **56(5),** 1138-1147.

6. DeLeon-Pennell KY, de Castro Brás LE, Lindsey ML (2013) Circulating *Porphyromonas gingivalis* lipopolysaccharide resets cardiac homeostasis in mice through a matrix metalloproteinase-9-dependent mechanism. *Physiol Rep* 1. 10.1002/phy2.79.

7. Troseid M, Nestvold TK, Rudi K, Thoresen H, Nielsen EW, Lappegard KT (2013) Plasma lipopolysaccharide is closely associated with glycemic control and abdominal obesity. *Diabetes care* **36,** 3627-3632.

8. Poole S, Singhrao SK, Kesavalu L, Curtis MA, Crean StJ (2013) Determining the presence of periodontopathic virulence factors in short-term postmortem Alzheimer's disease brain tissue. *J Alzheimers Dis* **36,** 665-677.

9. Dominy SS, Lynch C, Ermini F, Benedyk M, Marczyk A, Konradi A, Nguyen M, Haditsch U, Raha D, Griffin C, Holsinger LJ, Arastu-Kapur S, Kaba S, Lee A, Ryder MI, Potempa B, Mydel P, Hellvard A, Adamowicz K, Hasturk H, Walker GD, Reynolds EC, Faull RLM, Curtis MA, Dragunow M, Potempa J (2019) *Porphyromonas gingivalis* in Alzheimer's disease brains: Evidence for disease causation and treatment with small-molecule inhibitors. *Sci Adv* **5(1),** eaau3333.

10. Alzheimer A, Stelzmann RA, Schnitzlein HN, Murtagh FR (1995)An English translation of Alzheimer's 1907 paper, "Uber eine eigenartige Erkankung der Hirnrinde".*Clin Anat* **8(6),** 429-431.

11. Veerhuis R, Nielsen HM, Tenner AJ (2011) Complement in the brain. *Mol Immunol* **48(14),** 1592-603.

12. Kumar DK, Choi SH, Washicosky KJ, Eimer WA, Tucker S, Ghofrani J, Lefkowitz A, McColl G, Goldstein LE, Tanzi RE, Moir RD (2016) Amyloid-b peptide protects against microbial infection in mouse and worm models of Alzheimer's disease. *Sci Transl Med* **8,** 340ra72.

13. Eimer WA, Vijaya Kumar DK, Navalpur Shanmugam NK, Rodriguez AS, Mitchell T, Washicosky KJ, György B, Breakefield XO, Tanzi RE, Moir RD (2018) Alzheimer's Disease-Associated β-Amyloid Is Rapidly Seeded by Herpesviridae to Protect against Brain Infection. *Neuron* **99(1),** 56-63.e3. doi: 10.1016/j.neuron.2018.06.030

14. Díaz-Zúñiga J, More J, Melgar-Rodríguez S, Jiménez-Unión M, Villalobos-Orchard F, Muñoz-Manríquez C, Monasterio G, Valdés JL, Vernal R, Paula-Lima A (2020) Alzheimer's Disease-Like Pathology Triggered by Porphyromonas gingivalis in Wild Type Rats Is Serotype Dependent. *Front Immunol*. **11,** 588036. doi: 10.3389/fimmu.2020.588036. eCollection 2020.

15. Chaffee B, Weston S (2010) Association between chronic periodontal disease and obesity: a systematic review and meta-analysis. *J Periodontol* **81,** 1708-1724.

16. Campus G, Salem A, Uzzau S, Baldoni E, Tonolo G (2005) Diabetes and periodontal disease: a case-control study. *JPeriodontol* **76,** 418-425.

17. Mysak J, Podzimek S, Sommerova P, Lyuya-Mi Y, Bartova J, Janatova T, Prochazkova J, Duskova J (2014) *Porphyromonas gingivalis*: Major Periodontopathic Pathogen Overview. *JImmunol Res* 2014:476068.doi: 10.1155/2014/476068.

18. Chiu H-C, Fu MM.-J., Yang T-S, Fu E, Chiang C-Y, Tu H-P, Chin Y-T, Lin F-G, Shih K-C (2016) Effect of high glucose, *Porphyromonas gingivalis* lipopolysaccharide and advanced glycation end-products on production of interleukin-6/-8 by gingival fibroblasts. *J periodontal Res* 52. 268-276.

19. Murray DA, Wilton JM (2003) Lipopolysaccharide from the periodontal pathogen Porphyromonas gingivalis prevents apoptosis of HL60-derived neutrophils in vitro. *Infect Immun.* 71(12):7232-5. doi: 10.1128/iai.71.12.7232-7235.2003.

20. Holmes C, Cotterell D (2009) Role of infection in the pathogenesis of Alzheimer's disease. *CNS Drugs* **23(12),** 993-1002.

21. Marques F, Sousa JC, Sousa N, Palha JA (2013) Blood-brain-barriers in aging and in Alzheimer's disease. *Mol Neurodegener* 8: 38. doi: 10.1186/1750-1326-8-38.

22. van Oijen M, de Jong FJ, Witteman JC, Hofman A, Koudstaal PJ, Breteler MM (2007) Atherosclerosis and risk for dementia. *Ann Neurol* **61,** 403–410.

23. Demmer RT, Norby FL, Lakshminarayan K, Walker KA, Pankow JS, Aaron R Folsom AR, Mosley T, Beck J, Lutsey PL (2020) Periodontal disease and incident dementia: The Atherosclerosis Risk in Communities Study (ARIC). *Neurology* **95(12),** e1660-e1671.doi: 10.1212/WNL.0000000000010312.

24. Dioguardi M, Crincoli V, Laino L, Alovisi M, Sovereto D, Mastrangelo F, Russo LL, Muzio LL. (2020) The Role of Periodontitis and Periodontal Bacteria in the Onset and Progression of Alzheimer's Disease: A Systematic Review. *J Clin Med* 9(2):495. doi: 10.3390/jcm9020495

25. Li L, Cavuoto M, Biddiscombe K, Pike KE (2020) Diabetes mellitus increases risk of incident dementia in APOEε4 carriers: A meta-analysis. L. *J Alzheimer's Dis* **74(4),** 1295-1308.

26. Cole G, Neal JW, Singhrao SK, Jasani B, Newman GR (1993)The distribution of amyloid plaques in the cerebellum and brain stem in Down's syndrome and Alzheimer's disease: a light microscopical analysis. *Acta Neuropathol* **85(5),** 542-552.

27. Bahar B, Singhrao SK (2021) An evaluation of the molecular mode of action of trans-resveratrol in the Porphyromonas gingivalis lipopolysaccharide challenged neuronal cell model. *Mol biol Rep* **48(1),** 147–156.

28. Dennis G Jr, Sherman BT, Hosack DA, Yang J, Gao W, Lane HC, Lempicki RA (2003) DAVID: Database for Annotation, Visualization, and Integrated Discovery. *Genome Biol* **4(5),** P3.

29. Ilievski V, Zuchowska PK, Green SJ, Toth PT, Ragozzino ME, Le K, et al. (2018) Chronic oral application of a periodontal pathogen results in brain inflammation, neurodegeneration and amyloid beta production in wild type mice. *PLoS ONE* **13(10),** e0204941. https://doi.org/10.1371/journal.pone.0204941

30. Stein PS, Desrosiers M, Donegan SJ, Yepes JF, Kryscio RJ (2007) Tooth loss, dementia and neuropathy in the Nun study. *J Am Dent Assoc* **138(10),** 1314-1322.

31. Pandini G, Pace V, Copani A, Squatrito S, Milardi D, Vigneri R (2013) Insulin has multiple antiamyloidogenic effects on human neuronal cells. *Endocrinology* **154(1),** 375-87.

32. Cholerton B, Baker LD, Craft S (2013) Insulin, cognition, and dementia. *Eur J Pharmacol* **719**, 170–179.

33. Poole S, Singhrao SK, Chukkapalli S, Rivera M, Velsko I, Kesavalu L, Crean StJ (2015) Active infection of *Porphorymonas gingivalis* and infection-induced complement activation in ApoE-/-mice brains. *J Alzheimers Dis* **43(1),** 67-80.

34. Dunn N, Mullee M, Perry VH, Holmes C (2005) An association between dementia and infectious disease: evidence from a case-control study. *Alzheimer Dis Assoc Disord* **19(2),** 91-94.

35. Holmes C, El-Okl M, Williams AL, Cunningham C, Wilcockson D, Perry VH (2003) Systemic infection, interleukin 1beta and cognitive decline in Alzheimer's disease. *Neurol Neurosurg Psychiatry* **74(6),** 788-789.

36. Spinelli M, Fusco S, Grassi C (2019) Brain insulin resistance and hippocampal plasticity: Mechanisms and biomarkers of cognitive decline. *Front Neurosci* **13,** 788. doi: 10.3389/fnins.2019.00788.

37. Meloni AR, DeYoung MB, Lowe C, Parkes DG (2013) GLP-1 receptor activated insulin secretion from pancreatic β-cells: mechanism and glucose dependence. *Diabetes Obes Metab* **15(1),** 15–27.

38. Fu Z, Gong L, Liu J, Wu J, Barrett EJ, Aylor KW, Liu Z (2020) Brain Endothelial Cells Regulate Glucagon-Like Peptide 1 Entry Into the Brain via a Receptor-Mediated Process. *Front Physiol* **11,** 555. https://doi.org/10.3389/fphys.2020.00555

39. Knauf C, Cani PD, Perrin C, Iglesias MA, Maury JF, Bernard E, Benhamed F, Grémeaux T, Drucker DJ, Kahn CR, Girard J, Tanti JF, Delzenne NM, Postic C, Burcelin R (2005) Brain glucagon-like peptide-1 increases insulin secretion and muscle insulin resistance to favor hepatic glycogen storage. *J Clin Invest* **115(12),** 3554–3563.

40. Sandoval D, Sisley SR (2015) Brain GLP-1 and insulin sensitivity. *Mol Cell Endocrinol* **418 Pt 1,** 27–32.

41. Kuwabara T, Kagalwala MN, Onuma Y, Ito Y, Warashina M, Terashima K, Sanosaka T, Nakashima K, Gage FH, Asashima M (2011) Insulin biosynthesis in neuronal progenitors derived from adult hippocampus and the olfactory bulb. *EMBO Mol Med* **3,** 742–754.

42. Bedse G, Di Domenico F, Serviddio G, Cassano T (2015) Aberrant insulin signaling in Alzheimer's disease: current knowledge. *Front Neurosci* **9,** 204. https://doi.org/10.3389/fnins.2015.00204

43. Li X, Song D, Leng SX (2015) Link between type 2 diabetes and Alzheimer's disease: from epidemiology to mechanism and treatment. *Clin Interv Aging* **10,** 549–560.

44. de la Monte SM (2019) The Full Spectrum of Alzheimer's Disease Is Rooted in Metabolic Derangements That Drive Type 3 Diabetes. *Adv Exp Med Biol* **1128,** 45-83. doi: 10.1007/978-981-13-3540-2_4

45. Silha JV, Gui Y, Murphy LJ (2002) Impaired glucose homeostasis in insulin-like growth factor-binding protein-3-transgenic mice. *Am J Physiol Endocrinol Metab* **283(5),** E937-45. doi: 10.1152/ajpendo.00014.2002. PMID: 12376320.

46. Yarchoan M, Toledo JB, Lee EB, Arvanitakis Z, Kazi H, Han L-Y, Louneva N, Lee VM-Y, Kim SF, Trojanowski JQ, Arnold SE (2014). Abnormal serine phosphorylation of insulin receptor substrate 1 is associated with tau pathology in Alzheimer's disease and tauopathies. *Acta Neuropathol* **128,** 679–689.

47. Xu F, Na L, Li Y, Chen L (2020) Roles of the PI3K/AKT/mTOR signalling pathways in neurodegenerative diseases and tumours. *Cell Biosci* **10,** 54. doi: 10.1186/s13578-020-00416-0.

48. Gabbouj S, Ryhänen S, Marttinen M, Wittrahm R, Takalo M, Kemppainen S, Martiskainen H, Tanila H, Haapasalo A, Hiltunen M, Natunen T (2019) Altered insulin signaling in Alzheimer's disease brain - Special emphasis on PI3K-Akt Pathway. *Front Neurosci* **13,** 629. https://doi.org/10.3389/fnins.2019.00629

49. Antico Arciuch VG, Galli S, Franco MC, Lam PY, Cadenas E, Carreras MC, Poderoso JJ (2009) Akt1 intramitochondrial cycling is a crucial step in the redox modulation of cell cycle progression. *PLoS ONE* 4:e7523. doi: 10.1371/journal.pone.0007523.

50. Franke TF, Yang SI, Chan TO, Datta K, Kazlauskas A, Morrison DK, Kaplan DR, Tsichlis PN (1995) The protein kinase encoded by the Akt proto-oncogene is a target of the PDGF-activated phosphatidylinositol 3-kinase. *Cell* **2,** 727–736.

51. de La Monte SM (2014) Type 3 diabetes is sporadic Alzheimers disease: mini-review. *Eur Neuropsychopharmacol* **24,** 1954–1960.

52. Haditsch U, Roth T, Rodriguez L, Hancock S, Cecere T, Nguyen M, Arastu-Kapur S, Broce S, Raha D, Lynch CC, Holsinger LJ, Dominy SS, Ermini F (2020) Alzheimer's disease-like neurodegeneration in *Porphyromonas gingivalis* infected neurons with persistent expression of active gingipains. *J Alzheimer's Dis* **75,** 1361–1376.

53. Jope RS, Cheng Y, Lowell JA, Worthen RJ, Sitbon YH, Beurel E (2017) Stressed and inflamed, can GSK3 be blamed? *Trends Biochem Sci* **42,** 180–192.

54. Manolopoulos K, Klotz L, Korsten P, Bornstein SR, Barthel A (2010) Linking Alzheimer's disease to insulin resistance: the FoxO response to oxidative stress. *Mol Psychiatry* **15,** 1046–1052.

55. Jha NK, Jha SK, Kar R, Nand P, Swati K, Goswami VK (2019) Nuclear factor kappa β as a therapeutic target for Alzheimer's disease. *J Neurochem* **150,** 113-137.

56. O'Brien RJ, Wong PC (2011) Amyloid precursor protein processing and Alzheimer's disease. *Annu Rev Neurosci* **34,** 185–204.

57. Wójtowicz S, Strosznajder AK, Jeżyna M, Strosznajder JB (2020)The Novel Role of PPAR Alpha in the Brain: Promising Target in Therapy of Alzheimer's Disease and Other Neurodegenerative Disorders. *Neurochem Res* **45,** 972–988.

58. Beck JD, Moss KL, Morelli T, Offenbacher S (2018) Periodontal profile class is associated with prevalent diabetes, coronary heart disease, stroke, and systemic markers of C-reactive protein and interleukin-6. *J Periodontol* **89(2),** 157-165.

59. Leira Y, Carballo Á, Orlandi M, Aldrey JM, Pías-Peleteiro JM, Moreno F, Vázquez-Vázquez L, Campos F, D'Aiuto F, Castillo J, Sobrino T, Blanco J. (2020) Periodontitis and systemic markers of neurodegeneration: A case-control study. *J Clin Periodontol* **47(5),** 561-571.

60. Li A, Chen Y, van der Sluis LWM, Schuller AA, Tjakkes GH (2020) Mediation Analysis of White Blood Cell Count on the Association Between Periodontal Inflammation and Digit Symbol Substitution Test Scoring Cognitive Function Among Older U.S. Adults. *J Gerontol A Biol Sci Med Sci* glaa223. doi: 10.1093/gerona/glaa223.

61. Akiyama H, Barger S, Barnum S, Bradt B, Bauer J, Cole GM, Akiyama H, Barger S, Barnum S, Cooper NR, Eikelenboom P, Emmerling M, Fiebich BL, Finch

CE, Frautschy S, Griffin WS, Hampel H, Hull M, Landreth G, Lue L, Mrak R, Mackenzie IR, McGeer PL, O'Banion MK, Pachter J, Pasinetti G, Plata-Salaman C, Rogers J, Rydel R, Shen Y, Streit W, Strohmeyer R, Tooyoma I, Van Muiswinkel FL, Veerhuis R, Walker D, Webster S, Wegrzyniak B, Wenk G, Wyss-Coray T (2000) Inflammation and Alzheimer's disease. *Neurobiol Aging* **21,** 383-421.

62. Heneka MT, Carson MJ, El Khoury J, Landreth GE, Brosseron F, Feinstein DL, Jacobs AH, Wyss-Coray T, Vitorica J, Ransohoff RM, Herrup K, Frautschy SA, Finsen B, Brown GC, Verkhratsky A, Yamanaka K, Koistinaho J, Latz E, Halle A, Petzold GC, Town T, Morgan D, Shinohara ML, Perry VH, Holmes C, Bazan NG, Brooks DJ, Hunot S, Joseph B, Deigendesch N, Garaschuk O, Boddeke E, Dinarello CA, Breitner JC, Cole GM, Golenbock DT, Kummer MP (2015). Neuroinflammation in Alzheimer's disease. *Lancet Neurol* **14(4),** 388-405.

Table 1

Differential expression of genes caused by the *P. gingivalis* W83 (PG) induction of the db/db mice versus the *F. nucleatum* (FN) or sham infection in the cerebral hemisphere region of the brain (fold change values ≥ 2.0 and ≤− 2.0 folds in the *P. gingivalis* group and in the corresponding groups.

Gene	Location	Type of molecule	PG vs FN	PG/sham	FN/sham
Insulin like growth factor 1 (*IGF1*)	Extracellular space	Growth factor	+3.47	+2.25	-1.54
C-X-C motif chemokine ligand 10 (*CXCL10*)		Cytokine	+2.30	+1.78	-1.29
Interleukin 1 alpha (*IL1A*)		Cytokine	+2.22	+1.90	-1.17
Lymphotoxin alpha (*LTA*)		Cytokine	+2.17	+2.69	+1.24
Colony stimulating factor 1 (*CSF1*)		Cytokine	+2.13	+2.06	-1.03
Interleukin 1 beta (*IL1B*)		Cytokine	+2.07	+2.63	+1.27
Matrix metallopeptidase 2 (*MMP2*)		Peptidase	+3.35	+3.62	+1.08
Insulin degrading enzyme (*IDE*)		Peptidase	+2.19	+1.77	-1.24
Resistin (*RETN*)		Other	+6.11	+1.53	-3.99
insulin like growth factor binding protein 3 (*IGFBP3*)		Other	+3.42	+3.42	+1.00
C-reactive protein (*CRP*)		Other	+2.02	+2.56	+1.27
Toll like receptor 4 (*TLR4*)	Plasma membrane	Transmembrane receptor	+7.43	+7.21	-1.03
Interleukin 6 receptor (*IL6R*)		Transmembrane receptor	+6.05	+3.42	-1.77
Intercellular adhesion molecule 1 (*ICAM1*)		Transmembrane receptor	+5.32	+3.43	-1.55
interleukin 1 receptor type 2 (*IL1R2*)		Transmembrane receptor	+4.73	+2.27	-2.08
CD 80 molecule (*CD80*)		Transmembrane receptor	+2.78	+2.01	-1.39
CD 28 molecule (*CD28*)		Transmembrane receptor	+2.73	+1.93	-1.41
Vascular cell adhesion molecule 1 (*VCAM1*)		Transmembrane receptor	+2.15	+1.79	-1.20
Toll like receptor 6 (*TLR6*)		Transmembrane receptor	+2.15	+2.13	-1.01
Insulin like growth factor 1 receptor (*IGF1R*)		Transmembrane receptor	-3.01	-4.31	-1.43

Glucagon like peptide 1 receptor (*GLP1R*)		G-protein coupled receptor	+5.96	+2.07	-2.88
Glucagon like peptide 2 receptor (*GLP2R*)		G-protein coupled receptor	+4.61	+2.32	-1.99
C-C motif chemokine receptor 2 (*CCR2*)		G-protein coupled receptor	+3.67	+2.10	-1.74
Adenosine Receptor A1 (*ADORA1*)		G-protein coupled receptor	+2.03	+4.12	+2.03
Low density lipoprotein receptor (*LDLR*)		Transporter	+3.50	+3.48	-1.01
LDL receptor related protein 2 (*LPR2*)		Transporter	-3.08	-2.07	+1.49
Insulin receptor (*INSR*)		Kinase	+3.35	+1.33	-2.52
Kinase insert domain receptor (*KDR*)		Kinase	+2.89	+1.96	-1.47
Fibroblast growth factor receptor 4 (*FGFR4*)		Kinase	+2.58	+1.92	-1.35
Epidermal growth factor receptor (*EGFR*)		Kinase	+2.58	+1.26	-2.06
Protein tyrosine phosphatase receptor type C (*PTPRC*)		Phosphatase	+2.74	+1.63	-1.68
Angiostensin I converting enzyme (*ACE*)		Peptidase	+5.36	+3.47	-1.54
Dipeptidyl peptidase 4 (*DPP4*)		Peptidase	+2.21	+1.65	-1.34
Adenosine deaminase (*ADA*)		Enzyme	+2.88	+2.24	-1.28
Docking Protein 2 (*DOK2*)		Other	+4.90	+3.18	-1.54
Clathrin heavy chain (*CLTC*)		Other	+3.33	+2.76	-1.20
MTD88 innate immune signal transduction adaptor (*MYD88*)		Other	+2.08	+3.43	+1.65
Cyclase associated actin cytoskeleton regulatory protein 1 (*CAP1*)		Other	+2.05	+2.84	+1.38
Glycogen synthase 2 (*GYS2*)	Cytoplasm	Enzyme	+4.30	+6.42	+1.49
Hydroxysteroid 17-beta dehydrogenase 4		Enzyme	+2.42	+4.70	+1.94
KRAS proto-oncogene, GTPase (*KRAS*)		Enzyme	+2.30	+2.44	+1.06
Insulin receptor substrate 1 (*IRS1*)		Enzyme	+2.20	+1.93	-1.14
Nitric oxide synthase 2 (*NOS2*)		Enzyme	-4.64	-4.25	+1.09
Mitogen-activated protein kinase 7 (*MAPK7*)		Kinase	+3.75	+1.58	-2.37
Phosphoinositide-3-kinase regulatory subunit 2 (*PIK3R2*)		Kinase	+3.63	+2.23	+1.62

Component of inhibitor of nuclear factor kappa B kinase complex (*CHUK*)		Kinase	+3.38	+2.15	-1.57
ATP serine/threonine kinase 1 (*AKT1*)		Kinase	+2.87	+3.79	+1.32
Protein kinase cAMP-dependent type I regulatory subunit 1A (*PRKAR1A*)		Kinase	+2.74	+3.05	+1.11
Mitogen-activated protein kinase kinase kinase 1 (*MAP3K1*)		Kinase	+2.69	+1.65	-1.63
Protein kinase C beta (*PRKCB*)		Kinase	+2.58	+2.43	-1.06
Phosphoenolypyruvate carboxykinase 2, mitochondrial (*PCK2*)		Kinase	+2.56	+4.25	+1.66
Protein kinase cAMP-activated catalytic subunit alpha (*PRCAKA*)		Kinase	+2.55	+4.83	+1.90
Adenylate Kinase 2 (*AK2*)		Kinase	+2.45	+3.93	+1.61
Protein kinase C beta (*PRKCA*)		Kinase	+2.41	+2.32	-1.04
Raf-1 proto-oncogene, serine/threonine kinase (*RAF1*)		Kinase	+2.39	+2.63	+1.10
Phosphoinositide-3-kinase regulatory subunit 1 (*PIK3R1*)		Kinase	+2.37	+2.80	+1.18
Serum/glucocorticoid regulated kinase 1 (*SGK1*)		Kinase	+2.33	+1.68	-1.39
Interleukin 1 receptor associated kinase 4 (*IRAK4*)		Kinase	+2.25	+1.22	-1.85
Protein kinase C delta (*PRKCD*)		Kinase	+2.20	+2.23	+1.01
Serum/glucocorticoid regulated kinase 3 (*SGK3*)		Kinase	+2.13	+1.96	-1.09
Janus kinase 2 (*JAK2*)		Kinase	+2.13	+1.32	-1.62
Inhibitor of nuclear factor kappa B kinase subunit beta (*IKBKB*)		Kinase	+2.01	+2.66	+1.32
Caspase 7 (*CASP7*)		Peptidase	+2.53	+4.11	+1.62
Protein phosphatase 2 scaffold subunit A alpha (*PPP2R1A*)		Phosphatase	+2.08	+4.45	+2.14
Glucose 6 phosphatase catalytic subunit (*G6PC*)		Phosphatase	-2.53	-1.07	+2.37
Adenosine A2a receptor (*ADORA2A*)		G-protein coupled receptor	+2.34	+2.35	+1.01
Adenosine A2a receptor (*ADORA2B*)		G-protein coupled receptor	+2.12	+2.15	+1.01

Adaptor related protein complex 1 subunit sigma 2 (*AP1S2*)		Transporter	+3.90	+1.91	-2.04
Adaptor related protein complex 1 subunit sigma 1 (*AP1S1*)		Transporter	+2.29	+4.07	+1.78
Uncoupling protein 2 (*UCP2*)		Transporter	+2.18	+1.30	-1.68
Growth factor receptor bound protein 10 (*GRB10*)		Other	+4.05	+1.36	-2.97
Tubulin beta class I (*TUBB*)		Other	+2.68	+3.14	+1.17
GRB2 associated binding protein 1 (*GAB1*)		Other	+2.40	+2.08	-1.16
SOS Ras/Rho guanine nucleotide exchange factor 2 (*SOS2*)		Other	+2.27	+1.85	-1.23
Growth factor receptor bound protein 2 (*GRB2*)		Other	+2.14	+3.81	+1.78
CRK proto-oncogene, adaptor protein (*CRK*)		Other	+2.01	+2.51	+1.25
Suppressor of cytokine signaling 1 (*SOCS1*)		Other	-2.21	+1.49	+3.30
Forkhead box O1 (*FOXO1*)		Transcription regulator	+4.00	+3.35	-1.20
Nuclear factor kappa B subunit 2 (*NFKB2*)		Transcription regulator	+4.68	+3.77	-1.24
Nuclear factor of activated T cells 2 (*NFATC2*)		Transcription regulator	+2.82	+3.25	+1.15
Catenin beta 1 (*CTNNB1*)		Transcription regulator	+2.71	+1.91	-1.42
Fos proto-oncogene, AP-1 transcription factor subunit (*FOS*)		Transcription regulator	+2.71	+2.10	-1.29
Sterol regulatory element binding transcription factor 1 (*SREBF1*)		Transcription regulator	+2.69	+2.93	+1.09
Tumor protein p53 (*TP53*)		Transcription regulator	+2.62	+3.13	+1.20
Sterol regulatory element binding transcription factor 2 (*SREBF2*)		Transcription regulator	+2.31	+2.89	+1.25
Signal transducer and activator of transcription 3 (*STAT3*)		Transcription regulator	+2.31	+3.15	+1.36
Jun proto-oncogene, AP-1 transcription factor subunit (*JUN*)		Transcription regulator	+2.21	+3.35	+1.52
SMAD family member 7 (*SMAD7*)	Nucleus	Transcription regulator	+2.10	+1.74	-1.21
Cbl proto-ocogene (*CBL*)		Transcription regulator	+3.04	+1.59	-1.91

Signal transducer and activator of transcription 6 (*STAT6*)	Transcription regulator	-3.41	-2.23	+1.53
cAMP responsive element binding protein 1 (*CREB1*)	Transcription regulator	-4.76	-2.23	+2.13
Nuclear receptor subfamily 4 group A member 2 (*NR4A2*)	Ligand-dependent nuclear receptor	+2.45	+3.55	+1.45
Glycogen synthase kinase 3 beta (*GSK3B*)	Kinase	+4.78	+2.42	-1.97
APC regulator of WNT signaling pathway (*APC*)	Enzyme	+2.73	+1.26	-2.16
AE binding protein 1 (*AEBP1*)	Peptidase	+4.00	+2.29	-1.75
Cell division cycle 27 (*CDC27*)	Other	+2.34	+1.71	-1.37

Table 2

The major gene annotation clusters of gene ontology (GO) affected by the genes differentially expressed in the mice brain due to the *P. gingivalis* W83 induction compared to those infected with *F. nucleatum*.

Annotation	Enrichment score	GO term	Gene count	%	*P*-value
Cluster 1	7.970	GO:0006468~protein phosphorylation	25	26.32	1.3E-15
		GO:0016301~kinase activity	24	25.26	8.2E-13
		GO:0016310~phosphorylation	22	23.16	4.4E-12
		GO:0004672~protein kinase activity	20	21.05	4.8E-11
		GO:0035556~intracellular signal transduction	14	14.74	1.5E-07
		GO:0018105~peptidyl-serine phosphorylation	9	9.47	4.5E-07
		GO:0046777~protein autophosphorylation	10	10.53	4.6E-07
		GO:0004674~protein serine/threonine kinase activity	14	14.74	4.8E-07
		GO:0005524~ATP binding	23	24.21	1.2E-05
		GO:0000166~nucleotide binding	26	27.37	2.3E-05
		GO:0016740~transferase activity	22	23.16	2.9E-05
Cluster 2	4.060	GO:0006954~inflammatory response	13	13.68	2.2E-07
		GO:0006955~immune response	9	9.47	8.6E-05
		GO:0005125~cytokine activity	5	5.26	2.9E-02
Cluster 3	8.640	GO:0008286~insulin receptor signaling pathway	9	9.47	2.1E-10
		GO:0048009~insulin-like growth factor receptor signaling pathway	6	6.32	2.6E-09
		GO:0032869~cellular response to insulin stimulus	9	9.47	1.8E-08
Cluster 4	4.300	GO:0048009~insulin-like growth factor receptor signaling pathway	6	6.32	2.6E-09
		GO:0005159~insulin-like growth factor receptor binding	5	5.26	5.4E-07
		GO:0005158~insulin receptor binding	6	6.32	1.2E-06
		GO:0046326~positive regulation of glucose import	5	5.26	2.5E-05
		GO:0045725~positive regulation of glycogen biosynthetic process	4	4.21	5.9E-05

	GO:0014065~phosphatidylinositol 3-kinase signaling	4		4.21	2.9E-04
	GO:0043491~protein kinase B signaling	4		4.21	1.0E-03

Table 3
Canonical pathways affected by the *P. gingivalis* W83 (PG) infection of db/db mice versus either the *F. nucleatum* (FN) or sham infected brains.

Signaling pathways	Genes	PG/FN				PG/Sham				Sham/FN			
		Affected genes	Direction	Z-score	P-value	Affected genes	Direction	Z-score	P-value	Affected genes	Direction	Z-score	P-value
Inflammatory Cascade													
NF-kB	179	25	↑	+4.600	3.0e-32	23	↑	+4.379	3.7e-30	7	↓	-1.890	4.1e-10
Neuroinflammation	315	27	↑	+3.530	6.2e-29	23	↑	+2.711	2.2e-24	6	↓	-0.816	6.1e-07
LPS stimulated MAPK	83	14	↑	+3.207	1.5e-19	15	↑	+3.350	3.3e-22	0	↔	-	-
PI3K/AKT	189	20	↑	+1.500	2.4e-23	23	↑	+2.065	1.4e-29	3	↔	-	-
Toll-like receptor	77	12	↑	+3.000	1.8e-16	10	↑	+2.646	1.3e-13	3	↔	-	-
Interleukin 1	95	11	↑	+3.317	1.1e-13	9	↑	+3.000	4.2e-11	2	↔	-	-
Interleukin 6	126	20	↑	+4.472	5.0e-27	19	↑	+4.359	2.4e-26	3	↔	-	-
mTOR	216	10	↑	+2.530	1.3e-08	10	↑	+2.530	3.9E-09	2	↔	-	-
Diabetes													
Insulin-like growth factor1	106	20	↑	+3.771	1.2e-28	19	↑	+3.500	7.0e-28	3	↔	-	-
Insulin receptor	145	20	↑	+2.683	9.8e-26	16	↑	+2.000	5.1e-20	5	↓	-1.342	3.2e-07
Insulin secretion	267	13	↑	+2.496	3.9e-11	12	↑	+2.309	1.4e-10	5	↑	+0.447	6.5e-06
Type-2 diabetes	163	13	↑	+2.714	7.4e-14	11	↑	+2.530	1.1e-11	4	↔	-	-
Other													
PPAR	105	13	↓	-3.600	2.2e-16	15	↓	−3.873	1.4e-20	3	↔	-	-
PTEN	138	18	↓	-2.840	9.1e-23	16	↓	-2.673	2.2e-20	4	↔	-	-

Figure and legends

Figure 1

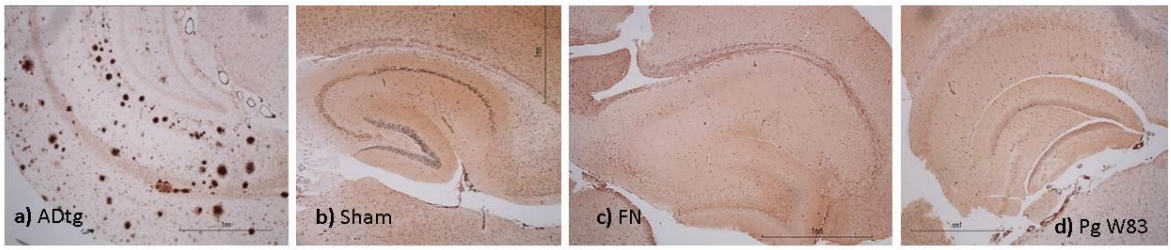

Figure 1

Rehydrated paraffin wax embedded brain tissue sections from the hippocampus of the AD transgenic Tg2576 (ADtg) mice and obese diabetic mice stained with methenamine silver to demonstateinsoluble amyloid-beta (Aβ) plaques.

a) AD transgenic mouse (positive control for Aβ plaques). Methenamine silver shows numerous argyrophilic plaques of variable size in the hippocampus in close proximity to the CA neurons. Some blood vessels stand out following silver impregnation.

b) Sham infected (sham) obese diabetic mice

c) *F.m nucleatum* (FN)

d) *P. gingivalis* (Pg W83), images b-d) from obese diabetic mice completely lacked Aβ plaques This image shows immunostaining with mouse anti-tau (AT8) antibody to detect neurofibrillary tangles.

Figure 2

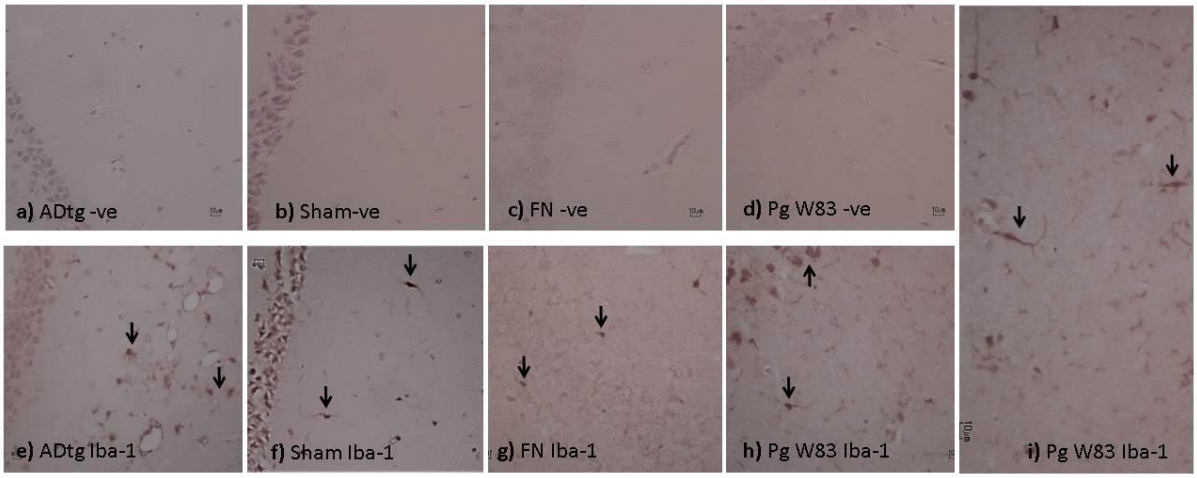

Figure 2

Rehydrated paraffin wax tissue sections and order of brains as for figure 1. This image shows immunostaining with rabbit anti-Iba-1 antibody to detect activated microglia.

Images a-d) show little staining as a negative control as when the primary antibody was omitted in all mice categories.

Images e-i) show variable degree of activated microglia scattered within the hippocampusas denoted by arrows. In the sham-infected (2f) and the *F. nucleatum* infected (2g) mice, showed only a few resting microglia. The *P. gingivalis* W83 mice demonstrated considerably more reactive microglial cell distribution with branched processes within the hippocampus (2h, I arrows).

Figure 3

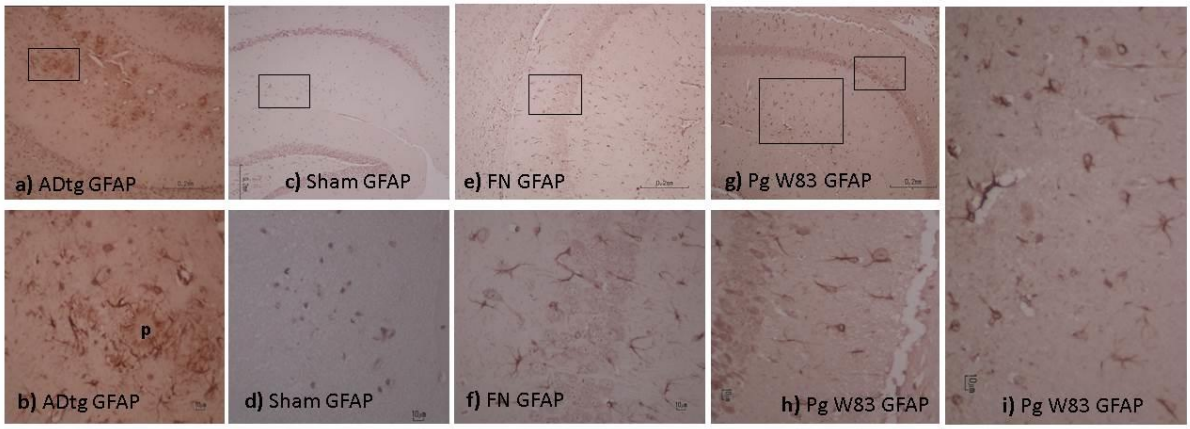

Figure 3

Rehydrated paraffin wax tissue sections and order of brains as for figure 1.

Immunolabelling of the GFAP

The AD trangenic mice brain sections (a-b) demonstrate numerous reactive astrocytes in close vicinity to the amyloid plaques (3a box, and b where p represents the amyloid plaque core and is the area within the box from 3a).

The sham brain sections (3c box, d area within the box in 3c) demonstrated resting astrocytes.

F. nucleatum infected mice hippocampus (e-f) demonstrated a significant numbers of activated astrocytes (3e box, f area within the box in 3e).

The *P. gingivalis* W83 brain sections, (3g box, h and i are areas from box in 3g) also demonstrated abundant reactive astrocytes.

Figure 4

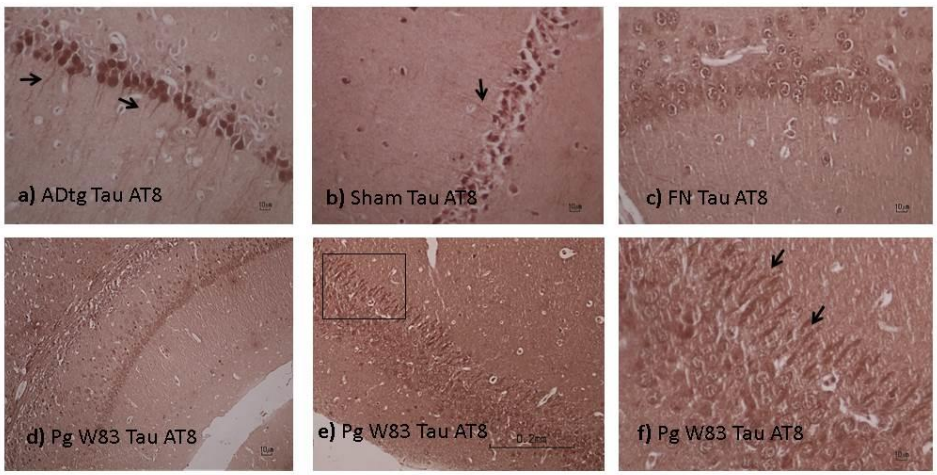

Figure 4

Rehydrated paraffin wax tissue sections and order of brains as for figure 1. This image shows immunostaining with mouse anti-tau (AT8) antibody to detect neurofibrillary tangles.

a) The AD trangenic mice exhibited an intense immunopositive staining within neurmerous CA neuronal cell bodies within the hippocampus. The axon hillock of some neurons was also immunostained (4a and arrows).
b) Sham infected mice demonstarted some inconspicuous stating in the axon hillock (4b and arrow).
c) In the *F. nucleatum* mice, a weak, largely diffuse tau immunostaining was observed within the CA neurons without evidence of staining within the axon hillock (4c).
d) The images d to f) are tissue sections from *P. ginivalis* W83 infected mice demonstrating tau immunostaining within the CA neurons and more stronger tau positive and thickened bundles of axon hillock(s) in the hippocampus (4d, e box, f arrows).

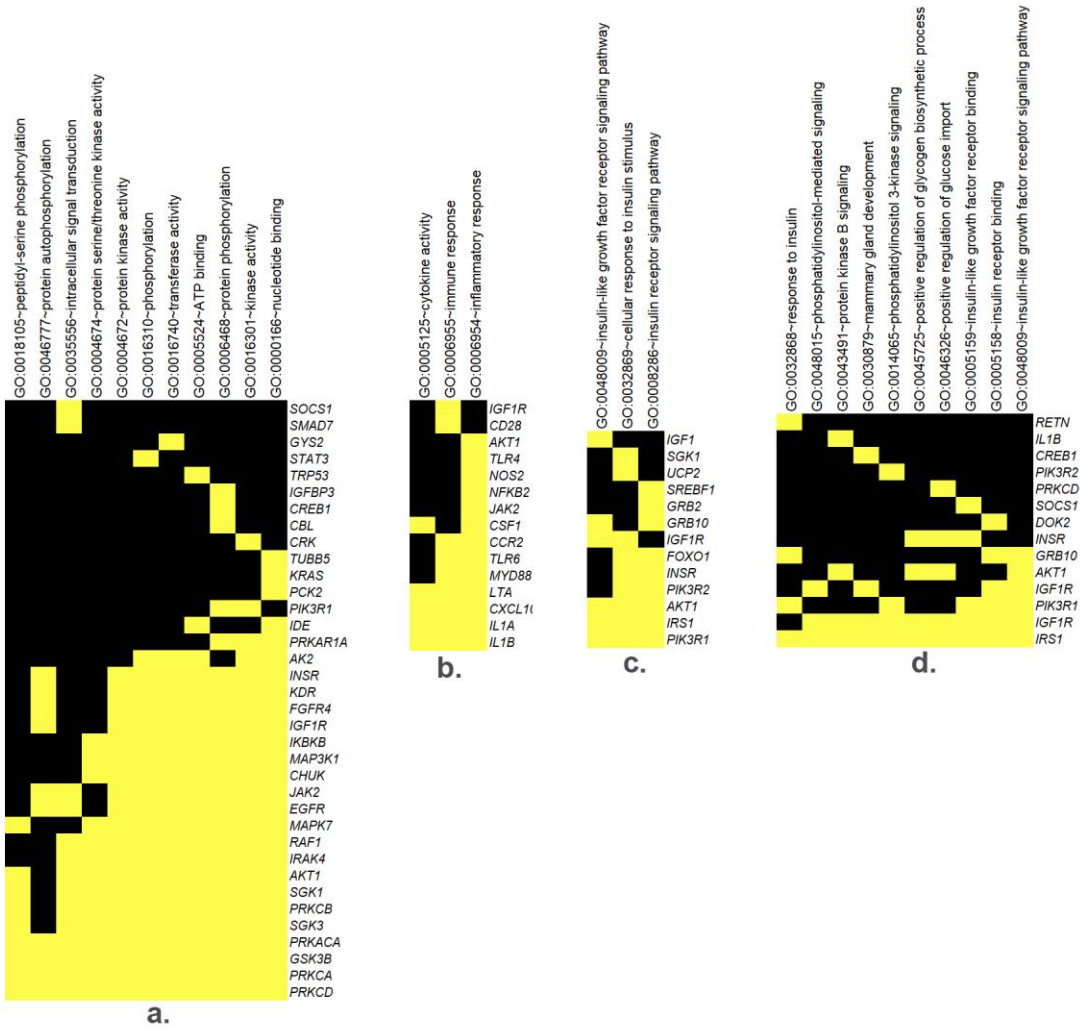

Figure 5

Gene annotation clusters of gene ontology (GO) term relating to kinases (a) and inflammatory immune response (b), insulin/IGF-1 signaling (c) and insulin/IGF-1 receptors (d) and the candidate gene/s associated with the GO term. The GO analysis was performed based on the 96 differentially expressed genes caused by the *P. gingivalis* W83 induction in the db/db mice compared to those treated with the *Fusobacterium nucleatum* (control). Two major clusters (Cluster 1 and 2) relating to kinases and inflammatory immune response and two clusters (cluster 3 and 4) relating to insulin/IGF-1signaling pathways are shown.

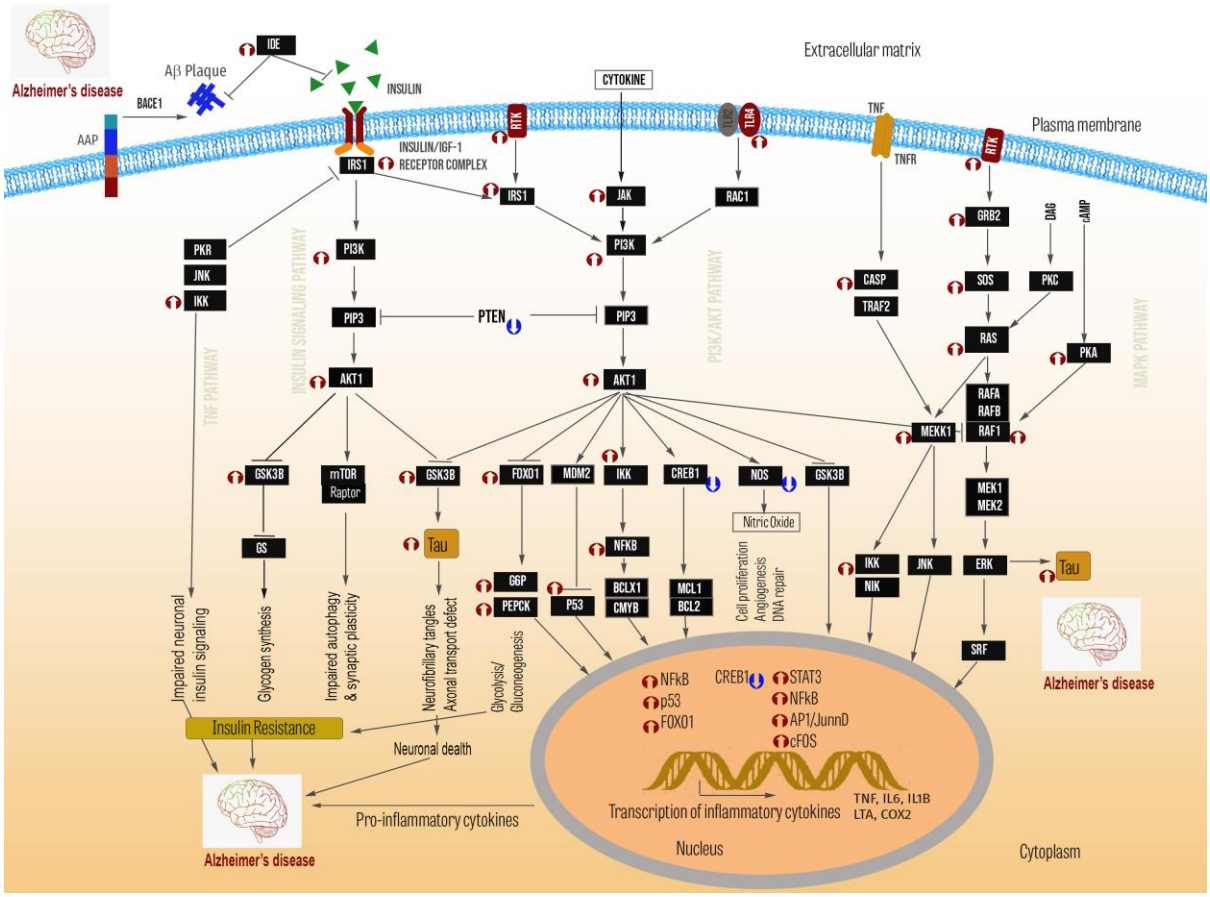

Figure 6

Schematic outline of four major pathways (PI3K/AKT pathway, MAPK pathway, Insulin signaling pathway and TNF pathway) affected in the db/db mice due to the *P. gingivalis* W83 induction. These interconnected pathways lead to altered activities of kinases (PI3K/AKT1, RAS/MEKK1)), affect insulin signaling (IRS1) and nutrient metabolism (AKT1), alter oxidative stress (NOS2), transcriptional activation pro-inflammatory genes (NFKB, AP1, cFOS), all potentially contributing to Alzheimer's disease pathophysiology (A□ plaque and Tau neurofibrillary tangles). The mRNA abundance of the markers as found in this study to increase (up arrow) or decrease (down arrow) following the *P. gingivalis* W83 treatment compared to those of the *F. nucleatum* infection are shown. The stimulatory and inhibitory relationship of the molecules are shown as arrow and hammer signs, respectively.